Journal of Mechanical Engineering and Sciences
ISSN (Print): 2289-4659; e-ISSN: 2231-8380
Volume 13, Issue 4, pp. 5735-5752, December 2019

DOI: https://doi.org/10.15282/jmes.13.4.2019.02.0458

Peridynamic model for nonlinear viscoelastic creep and creep rupture of Polypropylene

M. A. Azizi[1*], A. K. Ariffin[2]

[1] Department of Mechanical and Manufacturing Engineering, Faculty of Engineering, Universiti Putra Malaysia, 43400, Serdang, Selangor, Malaysia
[*]Email: muhdazim@upm.edu.my
Phone: +60136131202
[2] Faculty of Engineering and Build Environment, Universiti Kebangsaan Malaysia 43600, Bangi, Selangor, Malaysia

ABSTRACT

This paper presents the peridynamic numerical method for nonlinear viscoelastic creep behaviour which consists of primary, secondary, tertiary creep stages and creep rupture. A nonlinear viscoelastic creep constitutive equation based on internal state variable (ISV) theory which covers four creep stages is examined. The viscoelastic equation is substituted into material parameter in the peridynamic equation to derive a new peridynamic method with two time parameters i.e. numerical time and real time. The parameters of the viscoelastic equation is analyzed and evaluated. In validating this peridynamic method, a comparison is made between numerical and experimental data. The peridynamic method for nonlinear viscoelastic creep behaviour (VE-PD) is approved by the good similarity between numerical and experimental creep strain curves with overall difference of 10.67%. The nonlinearity of experimental and numerical data is adequately similar as the error between experimental and numerical curves of secondary stage strain rate against load is 8.022%. The shapes of fractured numerical specimen show good resemblance with the experimental result as well.

Keywords: peridynamic; viscoelastic; creep; polypropylene; nonlinear; fracture.

INTRODUCTION

Recently, fracture mechanic has been an important aspect in many fields of mechanical engineering researches. Automotive, aerospace, military machinery and building structure are the examples of fields that request for high expertise in fracture mechanic [1-4]. At the same time, viscoelastic material especially polymers and composites have been widely used due to their low weight but good strength performance. Therefore, further research on these material properties is required to increase their reliability [5-7]. One of the critical issues regarding the viscoelastic materials properties is the fracture behaviour of the materials. A recently introduced numerical method specialize in fracture mechanic i.e. peridynamic method is proposed in this work. Peridynamic method has good capability in simulating crack behaviours of materials because it has integral equation basis. The major contribution of this method is to overcome the disability of the conventional Finite Element Method (FEM)

which is unable to intrinsically simulate discontinuity such as crack and dislocation because it is based on differential equation. Extended Finite Element Method (XFEM) has been introduced to solve the discontinuity and remeshing problems but it still requires complex formulation to describe crack propagation behaviour [8-11]. Otherwise, peridynamic concept allows crack prediction without a need to intensively describe the crack propagation behaviour since the method itself allows intrinsic crack propagation. Failure occurs whenever and wherever it is energetically favourable [12, 13]. Presently, many peridynamic numerical tests on elastic fracture behaviour have been successfully conducted and the results were published in journals [14-17].

This paper is focused on application of peridynamic method on viscoelastic behaviour to achieve precise prediction of viscoelastic fracture behaviour. At the same time, the peridynamic method can be expanded into a new type of material i.e. viscoelastic material. Viscoelastic material consists of viscous and elastic properties. Viscoelastic material resists shear flow and strain linearly with time when stress is applied. It returns to original state with time-dependent manner once the stress is removed. In performing deformation test on viscoelastic material until rupture occur, viscoplastic behaviour which is closely related to viscoelastic behaviour should be considered. Viscoplasticity also called as nonlinear viscoelasticity is inelastic deformation behaviour that depends on the applied loading rate.

In creep test, specimen is applied with a constant load which is lower than the specimen ultimate tensile strength and the elongation of the specimen is monitored until rupture or until a certain time. Viscoelastic creep curve i.e. strain against time curve contains four main regions. The first region namely the initial strain is an immediate strain increase after load application. The initial strain is either purely elastic or combination of elastic and plastic parts. The second region namely primary creep stage is the region where the strain rate decreases with time until it reaches a stationary value. The third region namely secondary creep stage is the region with constant strain rate. The final region namely tertiary creep stage is the region with increasing strain rate until fracture occurs. All four viscoelastic creep regions can be simulated by using a nonlinear viscoelastic equation which based on internal state variable (ISV) theory [18]. This equation can also describe the nonlinearity of the material elongation against applied load in the creep test.

Finite Element Method has been used in viscoelastic creep behaviours simulations such as linear viscoelastic creep [19], nonlinear viscoelastic creep [20] and viscolastic creep fracture [21]. Linear and nonlinear viscoelastic behaviours consist of the four creep regions as mentioned above. Peridynamic method application on linear and nonlinear viscoelastic creep behaviours allows improved fracture prediction in viscoelastic creep fracture simulation. Peridynamic method application on linear viscoelastic creep behaviour without fracture has been done in previous research [22]. Beside creep test, an impact test on viscoelastic material by using peridynamic method has been accomplished by other researchers [23]. In this paper the peridynamic method are applied on nonlinear viscoelastic behaviour with fracture.

In Finite Element Method, the outcome of elastic static tensile test simulation is a single value of strain without time parameter. For numerical method with integral basis like peridynamic, the outcome of the same simulation is an endless fluctuation of strain value against the additional time parameter i.e. numerical time. The static value of the fluctuation can be obtained by calculating the steady state of the fluctuation. In viscoelastic creep test, a time parameter is exist due to the time-dependent behavour of the test where strain is

observed against time. The application of peridynamic method on viscoelastic creep behaviour produces a model with two time parameters i.e. real time and numerical time. Hence a suitable approach is needed to deal with the two time parameters issue.

PERIDYNAMIC FORMULATION AND MATERIAL MODELING

The main product in this research is the peridynamic model with nonlinear viscoelastic equation application. Initially, the peridynamic and viscoelastic formulations are studied. The bond force equation and material modulus in the peridynamic equation is examined. Then the viscoelastic equation is altered and adapted into the material modulus in the peridynamic equation. The nonlinearity feature of creep strain against applied load in the viscoelastic equation is studied and an appropriate nonlinearity formula is added to the peridynamic equation. Fracture behaviour is also added to the peridynamic equation by adding a ramp fracture equation.

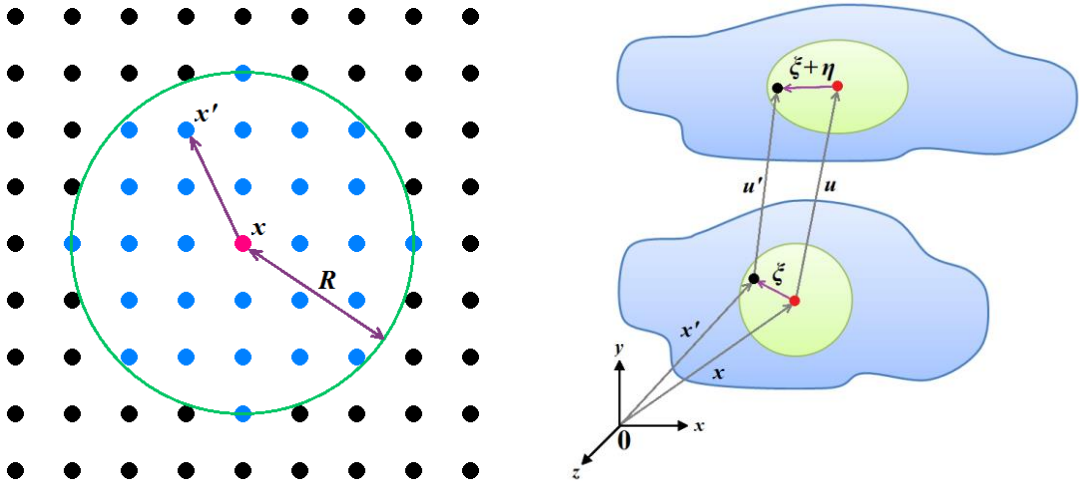

(a) (b)

Figure 1. (a) Horizon of a particle in peridynamic method and (b) Definition of $\boldsymbol{\xi}$ and $\boldsymbol{\eta}$ in peridynamic model.

The peridynamic formula as stated in Equation (1) is similar to the conventional finite element motion equation except for the bond-force equation i.e. the first component in Equation (1) where the conventional differential equation is replaced by an integral equation. This peridynamic motion equation has dimension of force per unit volume, F/V.

$$\rho \frac{\partial^2 \mathbf{u}}{\partial t^2} = \int_R dV_{x'} \mathbf{f}\left(\mathbf{u}(\mathbf{x},t), \mathbf{u}(\mathbf{x}',t), \mathbf{x}, \mathbf{x}', t\right) + \mathbf{b}(\mathbf{x},t) \qquad (1)$$

In peridynamic method, a particle, $\boldsymbol{x}$ only interacts with other particle, $\boldsymbol{x'}$ inside the horizon of the particle $\boldsymbol{x}$ as shown in Figure 1(a). The green circle with radius R is the horizon of particle $\boldsymbol{x}$ which is red in colour. The blue particles are the only particles that interact with particle $\boldsymbol{x}$ as the the particles are inside the horizon. The horizon in 3-dimensional model has spherical shape. The internal length, l is the parameter that decide the locality of the

interaction between particles. The interaction between particles becomes more local as the value of l reduced. The radius of the horizon, R is differing from 2 to 3 times the shortest distance between particles. This value range of R is used to ensure non-local behaviour of the numerical model. The vector $\boldsymbol{u}$ is the displacements of particles. The component **f** within the integral in equation (1) is the pairwise force function with unit of force per unit volume squared. Function **f** as in Equation (2) describes the force exerted by particle $\boldsymbol{x'}$ on particle $\boldsymbol{x}$. Matrix $\boldsymbol{\xi}$ is the initial distance between two nodes ($\boldsymbol{\xi} = \mathbf{x'} - \mathbf{x}$) and matrix $\boldsymbol{\eta}$ is the elongation of bond between two nodes ($\boldsymbol{\eta} = \mathbf{u}(\mathbf{x'},t) - \mathbf{u}(\mathbf{x},t)$) as shown in Figure 1(b) [24].

$$\mathbf{f}\left(\boldsymbol{\eta},\boldsymbol{\xi}\right) = \frac{\partial w}{\partial \boldsymbol{\eta}}\left(\boldsymbol{\eta},\boldsymbol{\xi}\right) \tag{2}$$

The micropotential, w is the energy in a single bond and has unit of energy per unit volume squared. The micropotential depends on the relative elongation vector, $\boldsymbol{\eta}$ only through the scalar distance between the two stretched points. The micropotential function for this scalar-valued deformation is:

$$\hat{w}\left(y,\boldsymbol{\xi}\right) = w\left(\boldsymbol{\eta},\boldsymbol{\xi}\right), \qquad y = \left|\boldsymbol{\eta}+\boldsymbol{\xi}\right| \tag{3}$$

Differentiating Equation (3) with respect to $\boldsymbol{\eta}$ and combine the outcome with Equation (2) leads to:

$$\begin{aligned}\mathbf{f}\left(\boldsymbol{\eta},\boldsymbol{\xi}\right) &= \frac{\partial \hat{w}}{\partial \boldsymbol{\eta}}\left(y,\boldsymbol{\xi}\right)\\ &= \frac{\partial\left(\left|\boldsymbol{\xi}+\boldsymbol{\eta}\right|\right)}{\partial \boldsymbol{\eta}}\, f\left(\left|\boldsymbol{\xi}+\boldsymbol{\eta}\right|,\boldsymbol{\xi}\right)\\ &= \frac{\boldsymbol{\xi}+\boldsymbol{\eta}}{\left|\boldsymbol{\xi}+\boldsymbol{\eta}\right|}\, f\left(\left|\boldsymbol{\xi}+\boldsymbol{\eta}\right|,\boldsymbol{\xi}\right)\end{aligned} \tag{4}$$

where f is the scalar-valued force function defined by:

$$f\left(y,\boldsymbol{\xi}\right) = \frac{\partial \hat{w}}{\partial y}\left(y,\boldsymbol{\xi}\right) \tag{5}$$

If the material of interest is isotropic, f from Equation (4) does not depend on the direction of $\boldsymbol{\xi}$**.** For simplicity, it can be assumed that the scalar bond force f depends only on the strain of the bond or the bond stretch, s. Hence f can be defined as:

$$f\left(\boldsymbol{\eta},\boldsymbol{\xi}\right) = c_1 s\left(\boldsymbol{\eta},\boldsymbol{\xi}\right), \; s = \frac{\left|\boldsymbol{\xi}+\boldsymbol{\eta}\right| - \left|\boldsymbol{\xi}\right|}{\left|\boldsymbol{\xi}\right|} \tag{6}$$

The constant c_1 is material deformation constant [24, 25]. Equation (6) is substituted into Equation. (4) to produce a pairwise force function as shown in Equation. (7). An additional exponential component is included in Equation. (7) to offer a numerical feature in which force applied by a particle to another particle is inversely proportional with the distance between the two particles [13, 26, 27]. Viscoelastic constitutive equation is substituted in the bond-force equation, specifically in the material constant c_1, to obtain bond with viscoelastic behavior.

$$\mathbf{f}\left(\boldsymbol{\eta},\boldsymbol{\xi}\right) = \frac{\boldsymbol{\xi}+\boldsymbol{\eta}}{\left|\boldsymbol{\xi}+\boldsymbol{\eta}\right|} e^{-\left(\frac{\left|\boldsymbol{\xi}\right|}{l}\right)^2} c_1 s \tag{7}$$

In this work, a nonlinear viscoelastic constitutive equation is used to replace c_1 in the peridynamic bond force equation. Nonlinearity of viscoelastic material means the strain of material is nonlinear with the applied stress. There are several types of nonlinear viscoelasticity namely high temperature nonlinearity, large deformation nonlinearity and material nonlinearity. Most polymers are treated as nonlinear viscoelastic material. In this paper, high temperature nonlinearity is not considered since the temperature is set to be constant at room temperature. A nonlinear viscoelastic equation is selected and the formula is based on irreversible internal state variable (ISV) thermodynamic theory.

The viscoelastic formula which developed by previous researchers [18] is capable of describing the four stages of creep deformation. In this formula, creep strain is the result of internal structural adjustment and different creep stages which go along with different thermodynamic properties in terms of flow potential function and energy dissipation rate. In primary and secondary creep stages, the thermodynamic state of the material system tends to equilibrate spontaneously. These stages can be described by kinetic equations of ISVs which can be derived by one single flow potential function, where the energy dissipation rate decreases gradually over time. For tertiary creep and fracture stages, multiple potentials are required to describe evolution of ISVs so that the thermodynamic state of material system tends to depart from the steady strain rate state.

In Rice thermodynamic theory, there are three dimensionless macroscale ISVs introduced i.e. γ, λ, and χ. The γ and λ are used to describe viscoelastic and viscoplastic intrinsic structural change respectively, and χ is used to account for the damage effect. The Rice irreversible ISV thermodynamics which based on a constrained equilibrium state assumes that the state of solid material at any given time can be described entirely by the stress, $\boldsymbol{\sigma}$ or strain, $\boldsymbol{\varepsilon}$, the temperature, θ, and a set of scalar internal state variables (γ, λ, and χ) which characterize the physical changes of microstructures of the material [28]. These four variables are referred as thermodynamic state variables.

The strain equation can be expressed in term of viscoelastic and viscoplastic strains as following

$$\boldsymbol{\varepsilon} = \boldsymbol{\varepsilon}^{ve} + \boldsymbol{\varepsilon}^{vp} \tag{8}$$

where

$$\kappa_e^{-1}\dot{\boldsymbol{\varepsilon}}^{ve} + B\boldsymbol{\varepsilon}^{ve} = w^2\boldsymbol{\sigma} \tag{9}$$

$$\dot{\boldsymbol{\varepsilon}}^{vp} = D_1\left[\dot{\boldsymbol{\lambda}}_1 + \left(1+b\boldsymbol{\chi}\right)\dot{\boldsymbol{\lambda}}_2 + b\boldsymbol{\lambda}_2\dot{\boldsymbol{\chi}}\right],\ D_1 = a_2 - 1/\sqrt{3} \tag{10}$$

The viscoelastic strain equation, $\boldsymbol{\varepsilon}^{ve}$ includes the initial elastic strain and hardening effect. Since hardening effect has already provided by viscoplastic strain equation, $\boldsymbol{\varepsilon}^{vp}$ as in Equation. (10), thus the viscoelastic strain equation can be replaced by initial elastic strain equation, $\boldsymbol{\varepsilon}^{e}$ with E_e as the elastic modulus:

$$\boldsymbol{\varepsilon}^{e} = \frac{\boldsymbol{\sigma}}{E_e} \tag{11}$$

In Equation. (10), the parameter λ_1, λ_2 and χ are used to describe the hardening effect, the softening effect and damage respectively. Parameters λ_2 and χ have symbiosis interaction

namely, χ evolves only when λ_2 develops. In one dimensional form, the λ_1, λ_2 and χ are ramp equations as shown below

$$\dot{\lambda}_1 = \kappa_1 D_2 \left\langle \sigma - \sigma_y - D_2^{-1} k \lambda_1 \right\rangle, \qquad D_2 = 1/\sqrt{3} - a_2 \tag{12}$$

$$\dot{\lambda}_2 = \kappa_2 \left\langle \frac{(1+b\chi)\sigma - \sigma_x}{\sigma_x} \right\rangle^p \tag{13}$$

$$\dot{\chi} = \kappa_3 e^{\chi} \left(\frac{b\lambda_2 \sigma}{\sigma_x} \right)^2 sign\left(\dot{\lambda}_2\right) \tag{14}$$

Both Macaulay's brackets in equations $\dot{\lambda}_1$ and $\dot{\lambda}_2$ are the ramp equation as following

$$\langle \mathrm{X} \rangle = \begin{cases} \mathrm{X} & \mathrm{X} > 0 \\ 0 & \mathrm{X} \le 0 \end{cases} \tag{15}$$

While the ramp equation in $\dot{\chi}$ equation is as below

$$sign(\mathrm{X}) = \begin{cases} 1 & \mathrm{X} > 0 \\ 0 & \mathrm{X} = 0 \\ -1 & \mathrm{X} < 0 \end{cases} \tag{16}$$

All other unknowns, κ_1, κ_2, κ_3, D_2, k, a_2, b and p are the parameters of the equation. Parameter σ_x is the mean internal stress [29]. These parameters can be evaluated by fitting the numerical creep curve with experimental creep data. The fitting method is explained in section 3.

The behaviour of nonlinear strain against applied load can be added into the viscoelastic equation by applying Ramberg-Osgood equation [30]. This equation as in Equation. (17) was originally created to describe the nonlinear relationship between stress and strain in materials near their yield points.

$$\varepsilon = \frac{\sigma_0}{E} + \alpha_2 \frac{\sigma_0}{E} \left(\frac{\sigma_0}{\sigma_y} \right)^{n-1} \tag{17}$$

The parameter σ_0 is the applied stress, E is the Young's Modulus, σ_y is the yield strength, α_2 and n are the temperature-dependent material constants. The first term in the formula accounts for the elastic part while the second term accounts for the plastic part. It is assumed that the nonlinearity of strain against applied load only occur at secondary and tertiary creep stages. The primary stage strain is assumed to behave linearly due to the low strain value. Therefore, the Ramberg-Osgood multiplier is added into the viscoelastic formula as a multiplier to constant, κ_2 which decides the strain rate of the secondary creep stage. As the result, only strains in secondary and tertiary stages behave nonlinearly against the applied load. The Ramberg-Osgood multiplier, M is the nonlinear part within Eq. (17) as following:

$$M = 1 + \alpha_2 \left(\frac{\sigma_0}{\sigma_y} \right)^{n-1} \tag{18}$$

where the constant stress, σ_0 and the Young's Modulus, E are excluded. In Equation. (10), parameter $\dot{\lambda}_1$ is a component of viscoplastic strain rate, $\dot{\varepsilon}^{vp}$ where it defines the secondary creep stage gradient. Since $\dot{\lambda}_1$ is directly proportional with the applied load as shown in Equation. (12), the nonlinear relation between gradient of secondary creep stage and the applied load in nonlinear creep experiment can be the measure of the nonlinearity of the material. Hence, the value of parameter σ_y, α_2 and n in Equation. (18) can be obtained by fitting curve of Equation. (18) with the experimental curve of secondary creep stage gradients against applied loads.

Peridynamic model with viscoelastic properties can be developed by substituting viscoelastic creep equations as in Equation. (8) to (18) into material constant c_1 in the peridynamic bond-force equation as in Equation. (7). The creep modulus function, α which is the function of strain to stress ratio ($\boldsymbol{\varepsilon}/\boldsymbol{\sigma}$) of this nonlinear viscoelastic equation must be derived so that it can be substituted properly into c_1. However, it is difficult to derive creep modulus function of this equation because the nonlinear equation consists of some ramp functions. For simplicity, this equation is calculated analytically to produce creep curve which consists of primary, secondary and tertiary stages. Then the analytical creep curve is set as reference for numerical test, by substituting the data of the curve into the creep modulus, α in the peridynamic bond-force equation. The time parameter in viscoelastic equation is considered as real time, t_R. An example of the analytical creep curve as the reference is shown in Figure 2(a). The analytical creep curve shows good similarity with an experimental creep data of polyethylene specimen of ASTM standard D638 under axial load of 18 MPa in Figure 2(b), where the primary creep, secondary creep and tertiary creep stages exist.

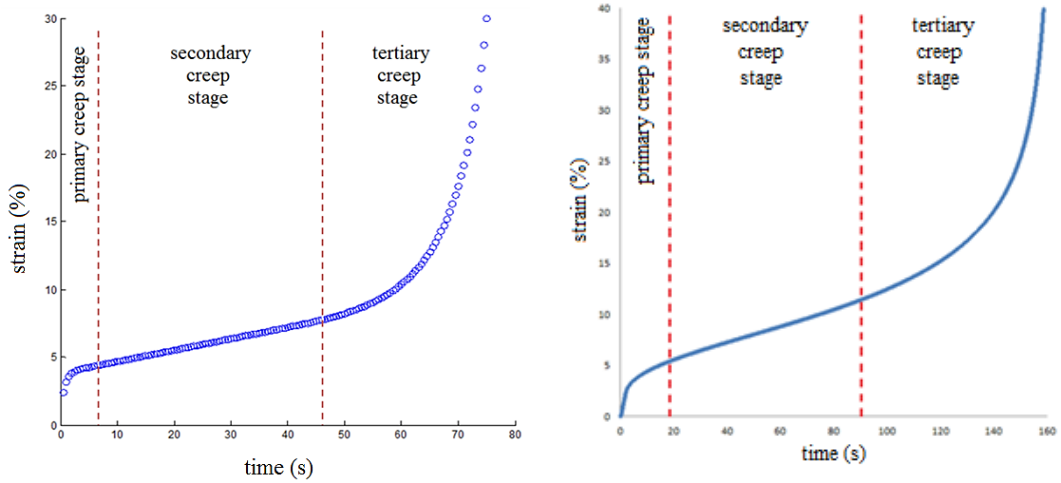

(a) (b)

Figure 2. (a) An example of analytical creep curve that used as numerical test reference. (b) An example of experimental creep curve of a viscoelastic material.

Critical strain is the value of strain at the transition from secondary stage to tertiary stage. It is noticed in experiment that at any value of load, the critical strain is approximately the same [31]. The viscoelastic equation however has a drawback where the critical strains of creep curves with different value of applied loads vary largely. Thus in this work the reference

creep curve is reformed where in the beginning there is no tertiary stage behaviour in the curve. The two damage equations, $\dot{\lambda}_2$ and $\dot{\chi}$ are initially deactivated to remove the tertiary stage behaviour. A critical strain value acquired from experimental data is applied. If strain of a bond reaches the critical strain, the damage equations ($\dot{\lambda}_2$ and $\dot{\chi}$) are initiated to add tertiary stage behaviour.

The response function i.e. Equation. (7) can be modified by adding a history-dependent scalar-valued function, μ to demonstrate fracture [32] as in following equation

$$\mathbf{f}\left(\boldsymbol{\eta},\boldsymbol{\xi}\right)=\frac{\boldsymbol{\xi}+\boldsymbol{\eta}}{\left|\boldsymbol{\xi}+\boldsymbol{\eta}\right|}e^{-\left(\frac{|\boldsymbol{\xi}|}{l}\right)^2}c_1 s\mu\left(\boldsymbol{\xi},t\right) \tag{19}$$

Where the function μ is described as:

$$\mu\left(\boldsymbol{\xi},t\right)=\begin{cases}1 & \text{if } s(t',\boldsymbol{\xi})<s_0 \text{ for all } 0<t'<t\\ 0 & \text{Otherwise}\end{cases} \tag{20}$$

in which s_0 is the fracture strain or fracture stretch. The value of s_0 is set by referring to experimental data. During numerical calculation, the strain of each bond is monitored continuously. When strain of a bond exceeds the value of s_0, the bond is ruptured and the two nodes that connected by the bond cease to interact with each other. Technically, as shown in Figure 3, the ruptured bond has μ equal to zero and hence the bond-force of the ruptured bond becomes zero as well. When the number of fractured bond increases and they are aligned, a crack appears and eventually a total fracture happened.

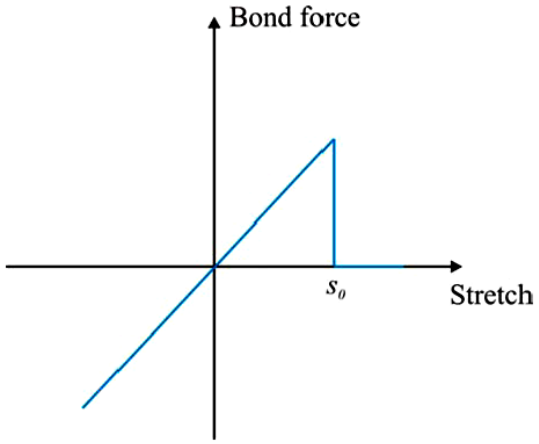

Figure 3. The relationship between bond-force and stretch of a bond and the effect of fracture stretch, s_0

The creep modulus, α is used to set the nonlinear constitutive viscoelastic creep equation into the peridynamic equation. The creep modulus is the ratio of strain to stress as in Equation. (21) which describes the elongation of viscoelastic material.

$$\alpha\left(t_R\right)=\frac{\varepsilon}{\sigma} \tag{21}$$

From Equation. (21), the scalar bond force function, f as stated in Equation. (6) can be obtained by using the stress equation, $\sigma = f/A$ where A is the cross-sectional area. The strain function is also elaborated in term of elongation, Δl and initial length, l_0

$$\alpha\left(t_R\right)=\frac{\Delta lA}{l_0 f} \tag{22}$$

Parameters Δl and l_0 in Equation. (22) are replaced with $|\boldsymbol{\eta}|$ and $|\boldsymbol{\xi}|$ respectively since they hold the same definition.

$$\alpha\left(t_R\right)=\frac{|\boldsymbol{\eta}|A}{|\boldsymbol{\xi}|f} \tag{23}$$

By arranging the bond force, f as the subject of Equation. (23), the following scalar viscoelastic bond-force equation is obtained:

$$f\left(\boldsymbol{\eta},\boldsymbol{\xi},t_R\right)=\frac{|\boldsymbol{\eta}|A}{|\boldsymbol{\xi}|\alpha\left(t_R\right)} \tag{24}$$

In Equation. (6), $f = c_1 s$. Since $s = |\boldsymbol{\eta}|/|\boldsymbol{\xi}|$, hence material constant, c_1 for time-dependent viscoelastic material is:

$$c_1\left(t_R\right)=\frac{A}{\alpha\left(t_R\right)} \tag{25}$$

Substitution of Equation. (25) into Equation. (7) derives a creep viscoelastic bond-force equation as shown below:

$$\mathbf{f}\left(\boldsymbol{\eta},\boldsymbol{\xi},t_R\right)=\frac{\boldsymbol{\xi}+\boldsymbol{\eta}}{|\boldsymbol{\xi}+\boldsymbol{\eta}|}e^{-\left(\frac{|\boldsymbol{\xi}|}{l}\right)^2}\left(\frac{A}{\alpha\left(t_R\right)}\right)s \tag{26}$$

The main difference of viscoelastic peridynamic bond-force equations from the elastic ones is the extra time parameter i.e. real time, t_R in the creep modulus, $\alpha(t_R)$. The value of A is unknown since there is no cross-sectional area between two nodes. For simplicity A is set as 1. This bond-force equation is for each connection between two nodes. In Equation. (1), the first component i.e. the integral equation sums all bond-force between node $\boldsymbol{x}$ and other nodes within horizon of node $\boldsymbol{x}$. The summed bond-force is then added with external forces, $\mathbf{b}(x,t)$ which include upward loads on the nodes at the top surface of specimen and all-direction fixtures on the nodes at the bottom surface of specimen. The outcome of the addition is the resultant force of node, $\boldsymbol{F_R}$ with unit of force per unit volume. From Equation. (1), the acceleration of node can be calculated by dividing the resultant force with the density of the material, ρ as following

$$\frac{\partial^2\mathbf{u}}{\partial t^2}=\frac{\mathbf{F}_R}{\rho} \tag{27}$$

NUMERICAL METHOD

Matrixes of $\mathbf{X}$, $\dot{\mathbf{X}}$ and $\ddot{\mathbf{X}}$ are introduced as matrix of position, velocity and acceleration of all nodes respectively. Matrix $\ddot{\mathbf{X}}$ includes acceleration, $\partial^2\boldsymbol{u}/\partial t^2$ as in Equation. (27) of all nodes. Index n is the counter of numerical time. As stated in equation (28), the combination of matrixes $\mathbf{X}$ and $\dot{\mathbf{X}}$ will form matrix $\mathbf{A}$ while combination of matrixes $\dot{\mathbf{X}}$ and $\ddot{\mathbf{X}}$ will form matrix $\mathbf{B}$. During the numerical process, the matrix of velocity and acceleration of time n, $\mathbf{B}_n$ is integrated by using Runge-Kutta (4,5) formula to obtain matrix of position and velocity of

time n+1, $\mathbf{A}_{n+1}$. The obtained position matrix is used to calculate the strain, s and then the resultant force, $\boldsymbol{F_R}$ of each bond by using Equation. (1) and (26). Then the acceleration of time n+1of each bond is calculated by dividing $\boldsymbol{F_R}$ with density, ρ as shown in Equation. (27). By placing the matrix of velocity and matrix of acceleration at time n+1 ($\dot{\mathbf{X}}_{n+1}$ and $\ddot{\mathbf{X}}_{n+1}$) in one matrix, $\mathbf{B}_{n+1}$ is produced. The cycle goes on until the computational time reach the finishing time, t_f.

$$\mathbf{A}_n = \begin{bmatrix} \mathbf{X}_n \\ \dot{\mathbf{X}}_n \end{bmatrix}, \mathbf{B}_n = \begin{bmatrix} \dot{\mathbf{X}}_n \\ \ddot{\mathbf{X}}_n \end{bmatrix} \tag{28}$$

$$\bar{\mathbf{A}}_m = \frac{\sum_n^{t_f} \mathbf{A}_n \left(t_{Rm} \right)}{t_f} \tag{29}$$

After the simulation process is finished, dynamic curve for each position and velocity (from matrix $\mathbf{A}_n$) against numerical time, t of each node is obtained. The mean values of the curves, $\bar{\mathbf{A}}_m$ are calculated as in Equation. (29). The index m is the counter for real time, t_R. All mean positions and velocities of nodes, $\bar{\mathbf{A}}_m$ at real times t_{R1}, t_{R2}, t_{R3}, ... , t_{Rf} i.e. $\bar{\mathbf{A}}_1$, $\bar{\mathbf{A}}_2$, $\bar{\mathbf{A}}_3$, ... , $\bar{\mathbf{A}}_{final}$ are calculated to obtain the complete strain against real time viscoelastic creep curve. The general computational process is described by the flow chart in Figure 4.

An averaging method from previous study is used to calculate the static value from the dynamic data [22]. The static value of particle position is calculated by adding all position values of all time points in the selected period, t_a as shown in Figure 5(a) and the sum is divided with the number of time step in the period. The value of t_a is the numerical time at the first peak of the dynamic data. The averaging process is repeated in every real time cycle (t_{R1}, t_{R2}, t_{R3}, ... , t_{Rf}) to obtain a complete creep curve. For an example, Figure 5(a) shows the position dynamic curve for each real time while Figure 5(b) shows the static values for all dynamic curves, plotted against real time to form a complete creep curve.

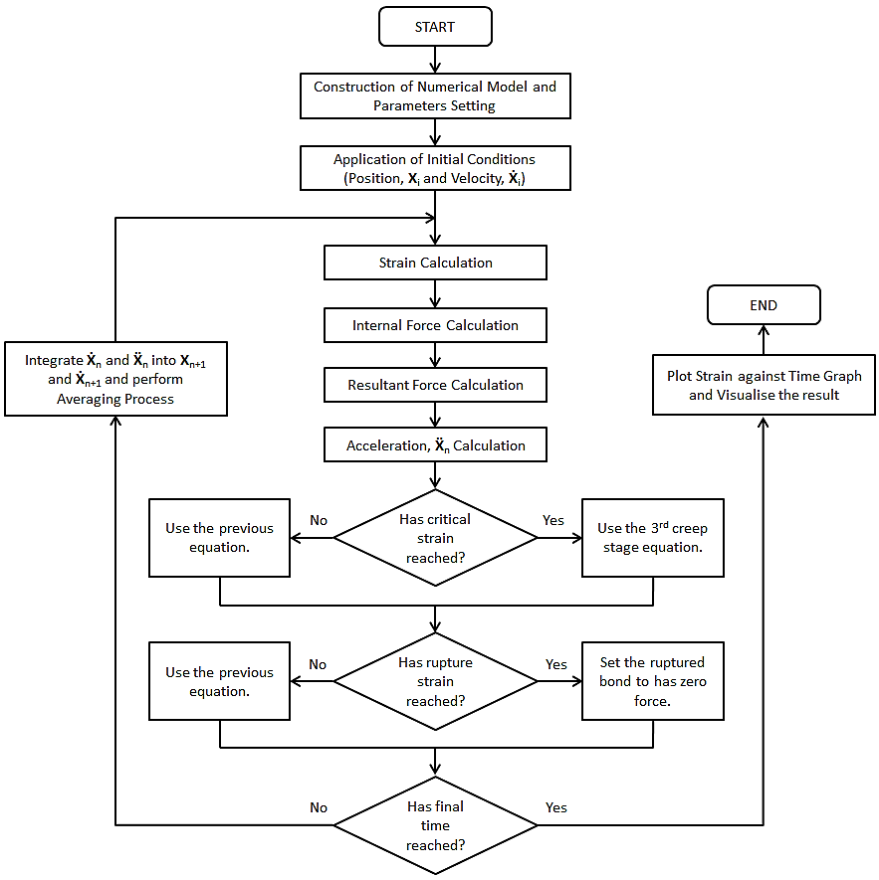

Figure 4. Flow chart of the peridynamic numerical process.

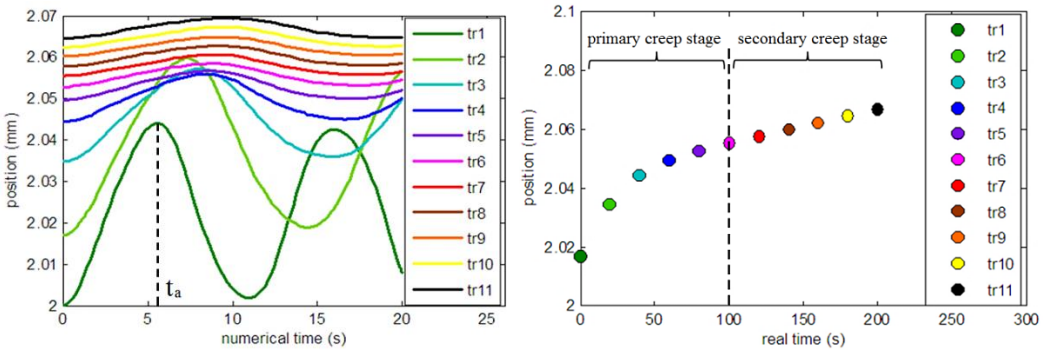

(a) (b)

Figure 5. (a) The dynamic curves of 11 values of real time, t_R=0s, 20s, 40s, 60s, 80s, 100s, 120s, 140s, 160s, 180s, 200s with an example of period t_a. (b) The average static position values of the dynamic curves against the real times that form a creep curve.

A previous research is referred in determining the values of peridynamic parameters i.e. the number of nodes per volume and the radius of horizon to obtain accurate numerical calculation [22]. The number of nodes per volume parameter can be denoted by node

intensity parameter, *a* which defined as minimum number of particle at sides of a model. From the paper, the optimal value of node intensity parameter, *a* is five particles for thick model and two particles for plate shape model. While the optimized value for horizon radius is three times the discretization value.

An error occurs due to the peridynamic non-local relation concept. Since a particle only interacts with other particles within the horizon, therefore inhomogeneity of strength occurs at surface of a model due to smaller number of connections of particle at the surface compare to particle at the middle of the model. This inhomogeneity problem can be ignored since the error is small and the effect can be lessened by increasing number of node. However, if the simulation only considers a specific section of a model where the other section is excluded for example gauge section as shown in Figure 6, the imaginary surfaces that connect the clamped section with the gauge have significant strength difference between numerical and experimental result due to the inhomogeneity problem. To solve this problem, all particles within horizon radius length from the imaginary surface are exempted from tertiary creep stage behaviour and rupture. This approach can avoid crack initiation at the imaginary surfaces and thus only applicable if there is no possibility for rupture to occur at the imaginary surfaces.

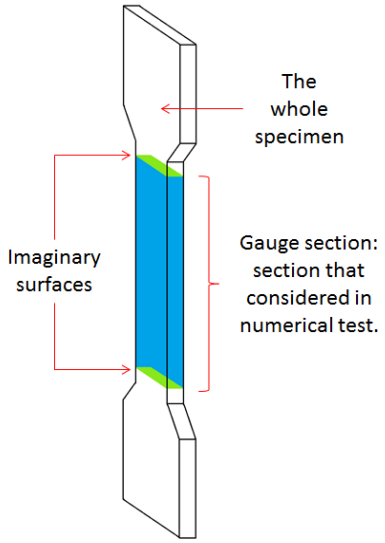

Figure 6. The green surface is the imaginary surface.

DETERMINATION OF VISCOELASTIC PARAMETERS

To compare experimental data with numerical data, a suitable creep experiment data from secondary source is used [31]. The material of the specimen is isotactic polypropylene Moplen HP 400R. The dimension of the specimen is based on ASTM standard D-638 and it is fabricated by using injection-molding machine Arburg 320C. The creep experiments are executed by using testing machine Instron-5569 at ambient temperature of 23ºC. The experimental result consists of six creep curves for six tests with different load values; 14.5 MPa, 19.7 MPa, 21.5 MPa, 22.7 MPa, 23.4 MPa, and 24.7 MPa. In the beginning of the test,

a sample was expanded with cross-head speed of 100 mm/min until a required stress value reached. Then the stress value is kept until the creep test complete. The specimen gauge dimensions are 50mm × 13mm × 3.2mm. In the numerical test, the model dimensions are set to be 33 units, 9 units and 2 units for length, width and thickness respectively, which is proportional with the actual specimen.

There are 12 material constants involved in the numerical calculation namely κ_1, κ_2, κ_3, k, a_2, b, σ_x, p, E_e, σ_y, α_2 and n. A fitting process between experimental curve and numerical curve is performed to obtain the values of the 12 constants. The experimental curve of load 22.7 MPa is made as reference for the fitting process. The fitting process is performed in a sequence where primary creep constants are evaluated first, followed by the secondary creep constants, tertiary creep constants, damage constant and finally the nonlinearity constants. For an example of optimization process, for constant k, an interval [0, k^o] is set where the best-fit of the constant is located in the interval. This interval is then divided into $J = 10$ sub-intervals by the point $k^{(i)} = i\Delta k$ with interval $\Delta k = k^o/J$ where $i = 0, 1, 2, \ldots, (J-1)$. Integration over time is performed by using Runge-Kutta (4,5) formula. Then least-square technique equation as following is used

$$F = \sum_{\alpha} \left[\varepsilon^{\exp}(t_\alpha) - \varepsilon^{num}(t_\alpha) \right]^2 \tag{30}$$

The summation in Equation. (30) is performed over all creep time, t_α. $\varepsilon^{\exp}$ is the engineering strain measured in experiment and ε^{num} is the strain value from the numerical simulation. The best-fit parameter k is found from the condition of minimum of function in Equation. (30). Next, the initial interval is replaced with a new smaller intervals [$k - \Delta k, k + \Delta k$] and the previous procedures are repeated. The best-fit values of the 12 constants were found by using the above-mentioned method and they are listed in Table 1.

Table 1. Adjustable parameters in the constitutive equations.

Parameter	**Optimized Value**	**Unit**
$\boldsymbol{\kappa_1}$	0.04	$(MPa.s)^{-1}$
$\boldsymbol{\kappa_2}$	0.3	$10^{-6}s^{-1}$
$\boldsymbol{\kappa_3}$	0.014	$10^{-5}s^{-1}$
$\boldsymbol{k}$	23.98	MPa
$\boldsymbol{a_2}$	0.201	-
$\boldsymbol{b}$	0.248	10^3
$\boldsymbol{\sigma_x}$	-120	kPa
$\boldsymbol{p}$	1.56	-
$\boldsymbol{E_e}$	360	MPa
$\boldsymbol{\sigma_y}$	0.529	MPa
$\boldsymbol{\alpha_2}$	7	-
$\boldsymbol{n}$	15	-

NUMERICAL-EXPERIMENTAL DATA COMPARISON

The polypropylene experimental creep data is obtained from a secondary resource [31]. The numerical creep curve in Figure 7 in overall shows adequate match with the experimental creep data. The percentage of error between experimental and numerical creep curves of load 14.5 MPa, 19.5 MPa, 21.5 MPa, 22.7 MPa, 23.4 MPa, and 24.7 MPa are 38.97%, 4.35%, 2.82%, 4.48 %, 2.5%, and 10.9% respectively. The average error for all loads is 10.67%. There is large error in creep curve of load 14.5 MPa. The tertiary stage of load 22.7 MPa, 23.4 MPa, and 24.7 MPa curves also display significant error with the experimental data.

The nonlinearity of strain against load can be measured from the curve of secondary creep stage gradient against applied load. Although the differences between experimental and numerical curves in Figure 7 are apparent, the nonlinear characteristics of the experimental and numerical data are pretty similar as shown in Figure 8. The average error of secondary stage strain rate against load between experimental and numerical data is 8.022%. In addition, the distribution of particles of numerical specimen after fracture shows good resemblance with fractured polypropylene specimen from self-performed creep experiment as shown in Figure 9. The necking exists in both experimental and numerical specimens. The scruffy fracture surfaces of numerical and experimental specimens show good similarity. Both numerical and experimental specimens also have crack surfaces with pointed tips. The main difference between the experimental and the numerical fractured specimens is the fracture location of the specimen.

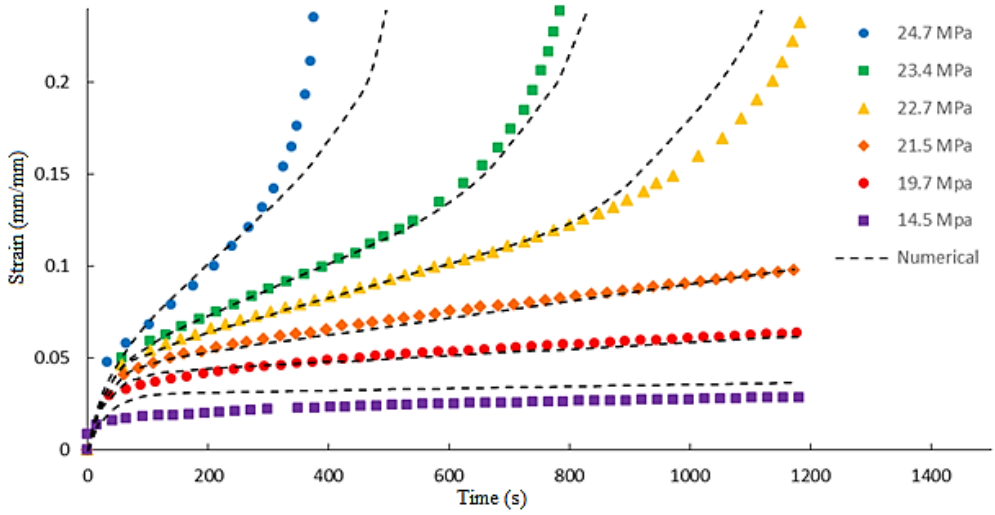

Figure 7. Comparison between experimental (polypropylene) and computational (peridynamic) creep tests.

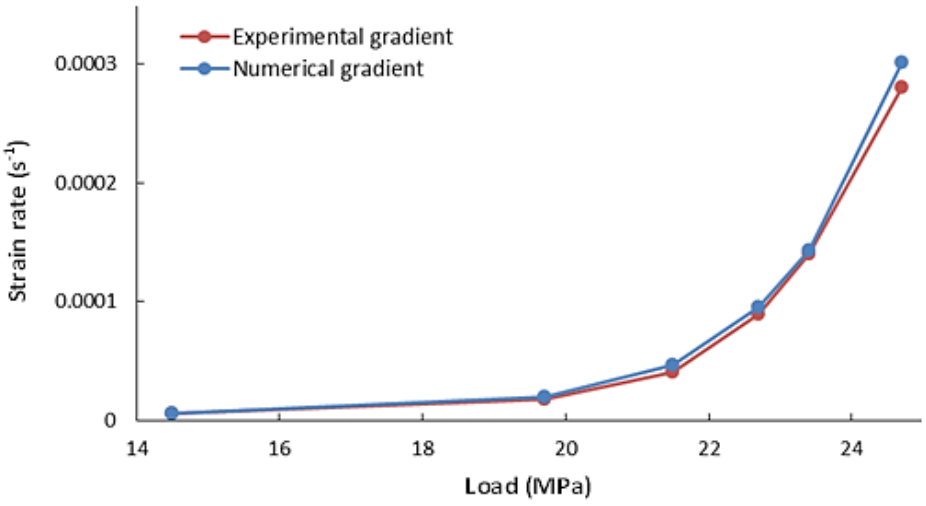

Figure 8. Curve of the strain rate of secondary creep stage against applied load.

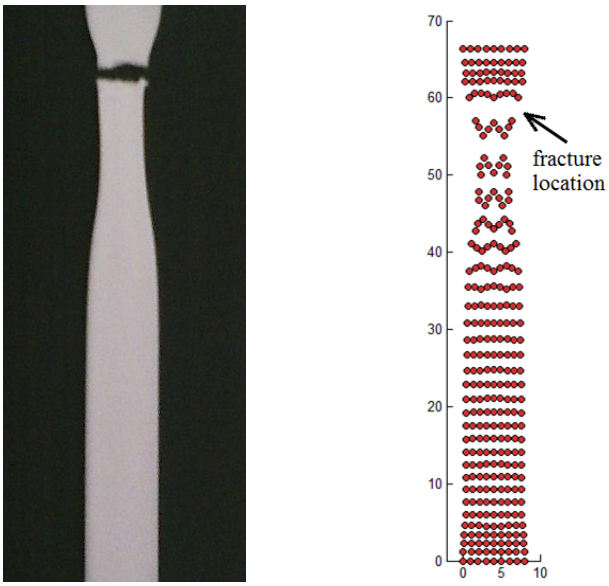

(a) (b)

Figure 9. (a) The shape of fractured experimental specimen due to creep test.
(b) Numerical specimen shape after creep test completed.

In the experimental result, the fracture can occur randomly along the gauge length but in the numerical results, the fracture consistently happens near to the load application location. This phenomenon occurred is due to the dynamic effect i.e. the load is applied dynamically to the specimen instead of statically. This issue is discussed in the next section.

The large difference between experimental and numerical curve of load 14.5 MPa is because of low nonlinearity of strain against applied load. Based on previous finding, if the strain is low and nearing 1%, the strain of the viscoelastic material tends to be more linear

with the applied load [31, 33]. The large error in the tertiary stage of load 22.7 MPa, 23.4 MPa and 24.7 MPa numerical curves is because of the higher nonlinearity in the tertiary stage than nonlinearity in the secondary stage in the experimental data. However, the nonlinearity of both secondary and tertiary stages is the same in numerical test. This assumption is confirmed by the bigger horizontal (time) separation of the three experimental tertiary stage curves than horizontal separation of the three numerical tertiary stage curves. These differences in nonlinear behaviour show that the nonlinearity of the strain against the applied load is increased as the strain increases. This claim is supported by the fact that stress of creep test is divided into two categories i.e. small stress and large stress, where the former is related to linear viscoelasticity and the latter related to nonlinear viscoelasticity [34]. Therefore, it is more accurate to use nonlinearity parameters values that change according to the applied load instead of using a single set of nonlinearity parameters values. This complex nonlinearity behaviour should be inspected further in order to obtain accurate prediction of viscoelastic creep, specifically in tertiary creep stage.

SUMMARY AND CONCLUSION

In summary, this work shows that peridynamic method is able to satisfactorily predict nonlinear viscoelastic creep behaviour which consist of the four creep stages and fracture by using the new viscoelastic equation based on internal state variable (ISV) theory. The notable difference between numerical and experimental data is mainly due to the change of nonlinearity behaviour. The nonlinearity of the secondary creep stage and the shape of fractured specimen have good similarities between numerical and experimental data. The subsequent work is to use enhanced nonlinear viscoelastic equation to have precise tertiary creep stage and creep fracture simulation. The fracture properties of viscoelastic material should be examined thoroughly in the future work. This current finding is first step of utilizing the main capability of peridynamic method upon viscoelastic material i.e. accurate prediction of crack properties such as crack propagation, crack initiation location and necking.

ACKNOWLEDGEMENTS

The authors would like to thank to the Universiti Putra Malaysia for financial assistance and to Universiti Kebangsaan Malaysia for providing computational and laboratory facilities.

REFERENCES

[1] Yoshimura T. Application of fracture mechanics on Japanese automotive industry. European Structural Integrity Society. 2000; 26:155-161.

[2] Wanhill RJH, Molent L, Barter SA. Fracture mechanics in aircraft failure analysis: Uses and limitations. Engineering Failure Analysis. 2013; 35:33-45.

[3] Nguyen DT, Nguyen VT. A fracture mechanics-based approach to modeling theconfinement effect in reinforced concrete column. Construction and Building Materials. 2016; 102: 893-903.

[4] Lyashuk O, Pyndus Y, Lutsiv I, Vovk Y, Poberezhna L, Tretiakov O, Zolotyy R. Fracture cause analysis of the extruder's shaft and geometry optimization of the spline. Journal of Mechanical Engineering and Sciences. 2019; 13(1): 4449-4460.

[5] Mayyas A, Qattawi A, Omar M, Shan D. Design for sustainability in automotive industry: a comprehensive review. Renewable and Sustainable Energy Reviews. 2012; 16:1845-1862.

[6] Wilson A. Vehicle weight is the key driver for automotive composites. Reinforced Plastics. 2015.

[7] Nordin MNA, Sakamoto K, Azhari H, Goda K, Okamoto M, Ito H, Endo T. Tensile and impact properties of pulverized oil palm fiber reinforced Polypropylene composites: A comparison study with wood fiber reinforced Polypropylene composites. Journal of Mechanical Engineering and Sciences. 2018; 12(4): 4191-4202.

[8] Xu Y, Yuan H. Application of normal stress dominated cohesive zone models for mixed-mode crack simulation based on extended finite element methods. Engineering Fracture Mechanics. 2011;78(3):544-558.

[9] Pourmodheji R, Mashayekhi M. Improvement of the extended finite element method for ductile crack growth. Materials Science and Engineering A. 2012; 551: 255-271.

[10] Zhang S, Wang G, Yu X. Seismic cracking analysis of concrete gravity dams with initial cracks using the extended finite element method. Engineering Structures. 2013; 6: 528-543.

[11] Brahma Raju K, Venkata Subbaiah K. Simulation of Ti-6Al-4V cruciform welded joints subjected to fatigue load using XFEM. Journal of Mechanical Engineering and Sciences. 2019; 13(3): 5371-5389.

[12] Hu W, Ha YD, Bobaru F. Peridynamic model for dynamic fracture in unidirectional fiber-reinforced composites. Computer Methods in Applied Mechanics and Engineering. 2012; 217-220 & 247-261.

[13] Oterkus E, Madenci E, Weckner O, Silling S, Bogert P, Tessler A. Combined finite element and peridynamic analyses for predicting failure in a stiffened composite curved panel with a central slot. Composite Structures. 2012; 94(3): 839-850.

[14] Kilic B, Madenci E. Structural stability and failure analysis using peridynamic theory. International Journal of Non-Linear Mechanics. 2009; 44(8): 845-854.

[15] Ha YD, Bobaru F. Characteristics of dynamic brittle fracture captured with peridynamics. Engineering Fracture Mechanics. 2011; 78(6): 1156–1168.

[16] Agwai A, Guven I, Madenci E. Crack propagation in multilayer thin-film structures of electronic packages using the peridynamic theory. Microelectronics Reliability. 2011; 51(12): 2298–2305.

[17] Wenke H, Yenan W, Jian Y, Chian-Fong Y, Florin B. Impact damage on a thin glass plate with a thin polycarbonate backing. International Journal of Impact Engineering. 2013; 62: 152-165.
[18] Zhang L, Liu Y, Yang Q. A creep model with damage based on internal variable theory and its fundamental properties. Mechanics of Materials. 2014; 78: 44-55.
[19] Gao D, Wang P, Li M, Luo W. Modelling of nonlinear viscoelastic creep behaviour of hot-mix asphalt. Construction and Building Materials. 2015; 95: 329-336.
[20] Paola MD, Scimemi GF. Finite element method on fractional viscoelastic frames. Computers and Structures. 2015; 164: 15-22.
[21] Nedjar B. Modeling long-term creep rupture by debonding in unidirectional fibre-reinforced composites. International Journal of Solids and Structures. 2014; 51: 1962–1969.
[22] Azizi MA, Ariffin AK, Nikabdullah N. The peridynamic model of viscoelastic creep and recovery. Multidiscipline Modeling in Materials and Structures. 2015; 11: 579-597.
[23] Weckner O, Nikabdullah N. Viscoelastic material models in peridynamics. Applied Mathematics and Computation. 2013; 219(11): 6039-6043.
[24] Kilic B, Madenci E. Peridynamic theory for thermomechanical analysis. IEEE Transaction on Advanced Packaging. 2010; 33(1): 97-105.
[25] Yi-le H, Yin Y, Hai W. Peridynamic analytical method for progressive damage in notched composite laminates. Composite Structures. 2014; 108: 801-810.
[26] Weckner O, Abeyaratne R. The effect of long-range forces on the dynamics of a bar. Journal of the Mechanics and Physics of Solids. 2005; 53(3): 705-728.
[27] Kilic B, Agwai A, Madenci E. Peridynamic theory for progressive damage prediction in center-cracked composite laminates. Composite Stuctures. 2009; 90(2): 141-151.
[28] Rice JR. Inelastic constitutive relation for solids: An internal variable theory and its application to metal plasticity. Journal of the Mechanics and Physics of Solids. 1971; 19: 433–455.
[29] Aubertin M, Gill DE, Ladanyi B. An internal variable model for the creep of rocksalt. Rock Mechanics and Rock Engineering. 1991; 24: 81–97.
[30] Irgens F. Chapter 9: Viscoelasticity. In: Irgens F. Continuum Mechanics. Girona: Springer-Verlag Berlin Heilderberg; 2008.
[31] Drozdov AD. Creep rupture and viscoelastoplasticity of Polypropylene. Engineering Fracture Mechanics. 2010; 77(12): 2277-2293.
[32] Silling SA, Askari E. A meshfree method based on the peridynamic model of solid mechanics. Computers and Structures. 2005; 83: 1526–1535.
[33] Gao L, Chena X, Gao H, Zhanga S. Description of nonlinear viscoelastic behavior and creep-rupture time of anisotropic conductive film. Materials Science and Engineering A. 2010; 527: 5115–5121.
[34] Ponnamma D, Thomas S. Origin of nonlinear viscoelasticity in filler rubbers: theory and practice. In: Ponnamma D, Thomas S. Viscoelasticity of Rubber Composites and Nanocomposites. Switzerland: Springer. 2014:1-13.